AGU100 ADVANCING EARTH AND SPACE SCIENCE

Geophysical Research Letters

RESEARCH LETTER
10.1029/2018GL077764

Abnormal Elasticity of Fe-Bearing Bridgmanite in the Earth's Lower Mantle

Suyu Fu[1], Jing Yang[1], Yanyao Zhang[1], Takuo Okuchi[2], Catherine McCammon[3], Hyo-Im Kim[4], Sung Keun Lee[4], and Jung-Fu Lin[1]

[1]Department of Geological Sciences, Jackson School of Geosciences, The University of Texas at Austin, Austin, TX, USA, [2]Institute for Planetary Materials, Okayama University, Misasa, Japan, [3]Bayerisches Geoinstitut, University of Bayreuth, Bayreuth, Germany, [4]School of Earth and Environmental Sciences, Seoul National University, Seoul, South Korea

Key Points:
- V_P and V_S of Fe-bearing bridgmanite $Mg_{0.96(1)}Fe^{2+}_{0.036(5)}Fe^{3+}_{0.014(5)}Si_{0.99(1)}O_3$ were measured up to 70 GPa at 300 K using BLS and ISLS
- The softening in V_P at ~42.6–58 GPa is consistent with the spin transition of B-site Fe^{3+} in bridgmanite
- Seismic heterogeneities in Fe-bearing bridgmanite could potentially occur in the mid-lower mantle in Fe-rich subducted slabs

Supporting Information:
- Supporting Information S1

Correspondence to:
J.-F. Lin,
afu@jsg.utexas.edu

Citation:
Fu, S., Yang, J., Zhang, Y., Okuchi, T., McCammon, C., Kim, H.-I., et al. (2018). Abnormal elasticity of Fe-bearing bridgmanite in the Earth's lower mantle. *Geophysical Research Letters*, *45*. https://doi.org/10.1029/2018GL077764

Received 2 MAR 2018
Accepted 2 MAY 2018
Accepted article online 8 MAY 2018

Abstract We measured the effect of pressure on the compressional and shear wave velocity (V_P, V_S) as well as density of Fe-bearing bridgmanite, $Mg_{0.96(1)}Fe^{2+}_{0.036(5)}Fe^{3+}_{0.014(5)}Si_{0.99(1)}O_3$, using impulsive stimulated light scattering, Brillouin light scattering, and X-ray diffraction, respectively, in diamond anvil cells up to 70 GPa at 300 K. A drastic softening of V_P by ~6(±1)% is observed between 42.6 and 58 GPa, while V_S increases continuously with increasing pressure. A significant reduction in Poisson's ratio from 0.24 to 0.16 occurs at ~42.6–58 GPa, while V_S increases by ~3(±1)% above ~40 GPa compared to $MgSiO_3$-bridgmanite. Thermoelastic modeling of the experimental results shows that the observed elastic anomaly of Fe-bearing bridgmanite is consistent with a spin transition of octahedrally coordinated Fe^{3+} in bridgmanite. These results challenge traditional views that Fe enrichment will reduce seismic velocities, suggesting that seismic heterogeneities in the mid-lower mantle may be due to a spin transition of Fe in Fe-bearing bridgmanite.

Plain Language Summary Seismic heterogeneities in the Earth's lower mantle have been attributed to thermal and/or chemical variations of constituent minerals. Bridgmanite is the most abundant lower-mantle mineral and contains Fe and Al in its structure. Knowing the effect of Fe on compressional and shear wave velocities (V_P, V_S) and density of bridgmanite at relevant pressure-temperature conditions can help to understand seismic heterogeneities in the region. However, experimental studies on both V_P and V_S of Fe-bearing bridgmanite have been limited to pressures below 40 GPa. In this study, V_P and V_S of Fe-bearing bridgmanite were measured up to 70 GPa in the diamond anvil cell. We observed drastic softening of V_P by ~6(±1)% at 42.6–58 GPa and increased V_S at pressures above 40 GPa. We interpret these observations as due to a spin transition of Fe^{3+}. These observations are different to previous views on the effect of Fe on seismic velocities of bridgmanite. We propose that the abnormal sound velocities of Fe-bearing bridgmanite could help to explain the seismically observed low correlation between V_P and V_S in the mid-lower mantle. Our results challenge existing models of Fe enrichment to explain the origin of Large Low Shear Velocity provinces in the lowermost mantle.

1. Introduction

Our understanding of the Earth's deep interior is based primarily on interpretation of seismic data using elastic and rheological properties of candidate minerals (e.g., Badro et al., 2005, Garnero & McNamara, 2008, Trampert et al., 2004). For example, thermal perturbation (higher temperature) is expected to lower velocity and density relative to the averaged mantle reference, while chemical perturbation, such as iron enrichment, is linked with increased density and reduced V_P and V_S (Garnero et al., 2016; Karato & Karki, 2001). Recent seismic studies have revealed large lateral velocity variations, referred to as seismic heterogeneities, in the middle part of the Earth's lower mantle, indicating thermal and/or chemical variations (ΔT, ΔX) in the region (e.g., Deschamps et al., 2007; Garnero et al., 2007; Masters et al., 2000; Simmons et al., 2010; Trampert et al., 2004; van der Hilst & Kárason, 1999). Furthermore, seismological observations have indicated a global disruption of fast V_P at ~1,700 km depth in the mid-lower mantle, which cannot be explained by temperature variations alone (Trampert et al., 2004; van der Hilst & Kárason, 1999). As a particular example of thermal and chemical variations in the deep mantle, two large low shear velocity provinces (LLSVPs) were observed beneath Africa and the Central Pacific regions at the base of the mantle, showing lower-than-average V_S (e.g., Garnero et al., 2016, Garnero & McNamara, 2008). LLSVPs can extend vertically as far up as 1,200 km above the core-mantle boundary (He & Wen, 2012; Tanaka et al., 2009) and are thus regarded as the most voluminous geological features of the Earth. The origin of LLSVPs has been attributed to either a higher-than-average temperature, Fe enrichment, or primordial material in the region (Davies et al., 2015; Fukui et al., 2016; Garnero et al., 2016; Lee et al., 2010). To better interpret these seismic observations in the lower mantle, comprehensive knowledge of chemical variation-induced velocity and density changes, especially due to Fe ($\partial V_{P,S}/\partial Fe$) and Al ($\partial V_{P,S}/\partial Al$) enrichment, of candidate lower-mantle minerals as a function of pressure-temperature (*P-T*) is critically needed.

Both geochemical and geophysical evidence indicate that (Al,Fe)-bearing bridgmanite [(Mg,Fe)(Al,Fe,Si)O_3] is the most abundant mineral in the Earth's lower mantle, accounting for ~75% in volume (e.g., Irifune et al., 2010; Kesson et al., 1998; Lin et al., 2013; Ringwood, 1975). Of particular relevance to interpreting the aforementioned thermal and chemical variations are the V_P, V_S and density profiles of (Al,Fe)-bearing bridgmanite at the relevant high *P-T* conditions of the lower mantle. Previous studies have shown that bridgmanite can accommodate as much as 10 mol.% Al, together with a substantial coupled substitution of Fe, about 11 mol.%, in its structure at mid-lower mantle conditions (Irifune et al., 2010; Xu et al., 2017). The incorporation of Fe in different spin and valence states in bridgmanite has been reported to influence its physical properties, such as elastic and transport properties (Chantel et al., 2012; Hsieh et al., 2017; Kurnosov et al., 2017; Li & Zhang, 2005; Liu et al., 2018; Mao et al., 2017; Murakami et al., 2012; Shukla et al., 2016; Wentzcovitch et al., 2004). While the thermal equation of state (EoS) of bridgmanite has been studied extensively (Boffa Ballaran et al., 2012; Dorfman et al., 2013; Lundin et al., 2008; Mao et al., 2017; Wolf et al., 2015), acoustic velocity results at high *P-T* are rare (Chantel et al., 2012; Jackson et al., 2005; Kurnosov et al., 2017; Li & Zhang, 2005; Murakami et al., 2007; Murakami et al., 2012). Thus far, experimental studies on both V_P and V_S of bridgmanite are still limited to pressures below 40 GPa due to technical limitations, such as the V_P peak of bridgmanite overlapping the diamond V_S peak at high pressure when using the Brillouin light scattering method. The influence of the Fe spin transition on the elasticity of Fe-bearing bridgmanite remains experimentally elusive. Further precise measurements on V_P, V_S and the density of Fe-bearing and (Al,Fe)-bearing bridgmanite at relevant *P-T* conditions of the lower mantle are critically needed to better understand seismic observations in the deep mantle.

Here we conducted Brillouin light scattering (BLS) and impulsive stimulated light scattering (ISLS) measurements on polycrystalline Fe-bearing bridgmanite $Mg_{0.96(1)}Fe^{2+}_{0.036(5)}Fe^{3+}_{0.014(5)}Si_{0.99(1)}O_3$ (Bgm5, $Fe^{3+}/\Sigma Fe = 0.28 \pm 0.06$) up to 70 GPa at room temperature in diamond anvil cells. These experimental results, together with synchrotron X-ray diffraction (XRD) data, are used to derive V_P, V_S, ρ, adiabatic bulk modulus (K_S), shear modulus (μ), and Poisson's ratio (ν) of the sample at lower-mantle pressures. Together with thermoelastic modeling, our results reveal the effects of the Fe spin transition on the elasticity of Fe-bearing bridgmanite at lower-mantle pressures. These results are further applied to understand possible seismic heterogeneities of the lower mantle that are caused by Fe chemical variation on V_P and V_S ($\Delta V_P/\Delta Fe$ and $\Delta V_S/\Delta Fe$) of lower-mantle bridgmanite.

2. Experiments

We synthesized polycrystalline bridgmanite (run number 5K2694) using Fe-bearing glass as the starting material at the Institute for Planetary Materials, Okayama University at Misasa (supporting information Text S1). The synthesized bridgmanite sample was measured using conventional Mössbauer spectroscopy at ambient conditions to determine the relative abundance of Fe^{2+} and Fe^{3+}. Analysis of the Mössbauer spectrum indicates that the sample contains 28(±6)% of Fe as Fe^{3+} (Figure S1). Based on the electron microprobe analysis and Mössbauer data, the sample was chemically homogeneous with a composition of $Mg_{0.96(1)}Fe^{2+}_{0.036(5)}Fe^{3+}_{0.014(5)}Si_{0.99(1)}O_3$. The formula is charge balanced with three oxygen atoms within experimental uncertainties. Based on these data and considering their respective precision limitations, Fe^{2+} occupies the A site while the site occupancy of Fe^{3+} could not be unambiguously determined from these data. XRD measurements of the sample at ambient conditions were conducted, affirming well-crystallized polycrystalline bridgmanite with orthorhombic structure (*Pbnm*) and lattice parameters a = 4.7832(4) Å, b = 4.9515(3) Å, and c = 6.9011(5) Å (Figures S2 and S3 in the supporting information). Scanning electron microscope and electron backscattered diffraction experiments were conducted on Bgm5 sample to determine its grain size and grain orientations, respectively, in the Electron Microbeam Laboratories of the Department of Geological Sciences at The University of Texas at Austin. Analysis of the scanning electron microscope results indicates that the Bgm5 typically has a grain size of ~2–4 μm and the electron backscattered diffraction patterns show

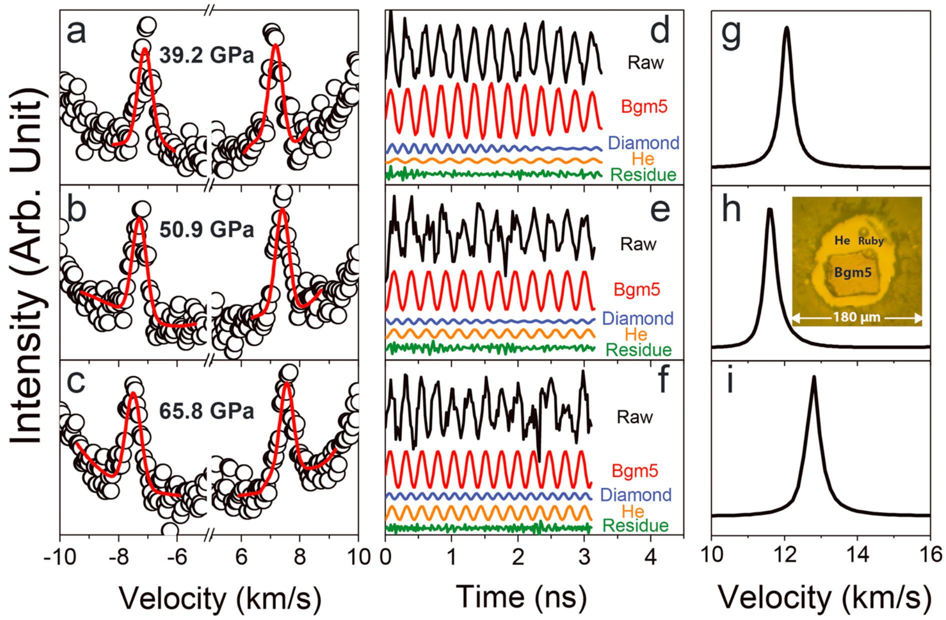

Figure 1. Representative Brillouin light scattering, impulsive stimulated light scattering, and power spectra of polycrystalline bridgmanite $Mg_{0.96(1)}Fe^{2+}_{0.036(5)}Fe^{3+}_{0.014(5)}Si_{0.99(1)}O_3$ (Bgm5) at high pressures and 300 K. (a–c) In Brillouin spectra, open black circles are experimental data and red lines show fitted spectra for V_S. Fourier transformation was employed on the collected time domain (d–f) impulsive stimulated light-scattering spectra to derive the (g-i) frequency domain power spectra and the V_P of the sample at corresponding pressures (see supporting information for detailed data analysis). The insert in Figure 1h shows a representative sample chamber image with Bgm5, a ruby sphere as the pressure calibrant and helium pressure medium at 50.9 GPa.

the sample to have grains with randomly distributed orientation without apparent texture or crystallographic preferred orientation (supporting information Figures S4 and S5).

High-pressure BLS and ISLS measurements were performed on the polycrystalline Bgm5 sample up to 70 GPa in a short symmetric DAC in the Mineral Physics Laboratory of the Department of Geological Sciences at The University of Texas at Austin. A 250 μm thick Re gasket was preindented to 42 μm thick using a pair of diamond anvils with 300-μm culets. A hole with a diameter of 190 μm was drilled into the preindented area to be used as the sample chamber. A Bgm5 platelet with a diameter of 70 μm was polished on both sides to 20-μm thickness and then loaded into the chamber. We conducted two high-pressure runs for BLS and ISLS: in the first run (Run 1), neon was used as the pressure medium up to 52 GPa, while helium, which provides conditions closer to hydrostatic, was used as the pressure medium up to 70 GPa in the second run (Run 2). A small ruby sphere was used as the pressure calibrant and was placed in each chamber adjacent to the sample (Dewaele et al., 2008; Mao et al., 1986). Pressure uncertainties were estimated from analysis of the measured ruby fluorescence spectra before and after experiments. Bridgmanite is stable at pressures above approximately 23 GPa, and thus, the pressure of the loaded samples was increased to 24 GPa for BLS and ISLS measurements in order to avoid potential sample degradation due to laser radiation at pressures below its stability field. Detailed setups of the BLS and ISLS system are described in supporting information Text S2 (Fu et al., 2017; Yang et al., 2015). Collection of BLS and ISLS spectra typically took ~1–2 hr and ~4–6 hr, respectively. Pressure intervals for the measurements were ~4–6 GPa at pressures below 40 GPa and ~1–2 GPa above 40 GPa. Analysis of the measured BLS and ISLS spectra was performed to determine V_S and V_P, respectively, of the sample at high pressures (Figures 1, S7, and S8).

3. Results and Discussion

Both V_S and V_P of Bgm5 were obtained up to 70 GPa in diamond anvil cells using the combination of BLS and ISLS techniques (Figure 2 and Table S1). Brillouin spectra show strong symmetric V_S peaks with high signal-to-noise ratio and high-quality V_P could be derived from analysis of the impulsive spectra at high pressures (Figures 1, S7, and S8). These results show that V_S increases monotonically across the whole experimental range, while V_P shows a significant softening between 42.6 GPa and 58 GPa, but then increases again with

10.1029/2018GL077764

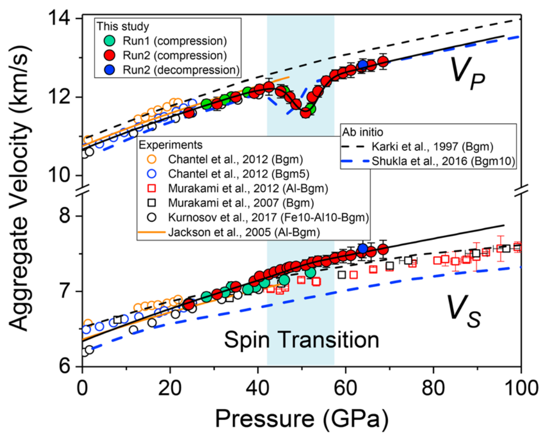

Figure 2. Aggregate compressional and shear wave velocities (V_P, V_S) of polycrystalline bridgmanite $Mg_{0.96(1)}Fe^{2+}_{0.036(5)}Fe^{3+}_{0.014(5)}Si_{0.99(1)}O_3$ (Bgm5) as a function of pressure at 300 K. Solid circles are experimental data from two runs, where the cell was loaded with neon in the first run (Run 1, green circles) and loaded with helium in the second run (Run 2, red circles), and blue circles are results from Run 2 during decompression. Solid black lines are modeled velocity profiles of Run 2 using thermoelastic equations. Data from Run 2 in He medium were used in the thermoelastic modeling (Run 1 data were not used because of suspected nonhydrostaticity at higher pressures; see supporting information for details). Previous literature results on bridgmanite with different compositions are plotted for comparison. References are shown in the legend. The softening of V_P at 42.6–58 GPa in this study is consistent with theoretical predictions in Fe-bearing bridgmanite [$(Mg_{0.95}Fe_{0.05})(Si_{0.95}Fe_{0.05})O_3$, Bgm10] across the spin transition of B-site Fe^{3+} at high pressures (blue dashed line) (Shukla et al., 2016), but our observed V_P softening with 1.5 mol.% Fe^{3+} in bridgmanite sample is much more profound. Uncertainties are smaller than symbols when not shown.

pressure up to 70 GPa. At pressures below 30 GPa, both V_P and V_S of our Bgm5 sample are consistent, within uncertainty, with an earlier ultrasonic study on bridgmanite with composition $Mg_{0.95}Fe^{2+}_{0.04}Fe^{3+}_{0.01}SiO_3$ (Chantel et al., 2012). However, above 40 GPa, the V_S determined for Bgm5 is 3%–4% higher than that measured using BLS for pure $MgSiO_3$-bridgmanite as well as Al-bearing bridgmanite containing 4 wt % Al_2O_3 (Murakami et al., 2007, 2012). On the other hand, V_P of Bgm5 is up to ~10% lower than the extrapolated value for pure $MgSiO_3$-bridgmanite between 42.6 and 58 GPa (Chantel et al., 2012; Karki et al., 1997). Based on the measured V_S and V_P, we have calculated the aggregate K_S and μ of Bgm5 at high pressure using the following equations:

$$K_S = \rho\left(V_P^2 - \frac{4}{3}V_S^2\right) \quad (1)$$

$$\mu = \rho V_S^2 \quad (2)$$

where ρ is the density of the sample under the corresponding pressures, which were obtained from complementary XRD results. The derived values of K_S and μ below 42.6 GPa are in good agreement with previous studies on (Al,Fe)-bearing bridgmanite (Figure 3a) (Chantel et al., 2012; Jackson et al., 2005; Kurnosov et al., 2017), while Ks softens drastically by 25(±4)% between 42.6 and 58 GPa. We note that the results between Run 1 and Run 2 using Ne and He as pressure medium, respectively, are consistent with each other at pressures below 38 GPa, while there is a slight difference at higher pressures up to 52 GPa. Such a difference might arise from deviatoric stress in the Ne pressure medium at higher pressures. Therefore, all discussion and modeling in this study are based on the experimental data from Run 2 using the He pressure medium.

In order to further decipher the thermoelastic behavior of Bgm5 at high pressure, third-order Eulerian finite-strain equations were used to derive K_{S0} and μ_0 at ambient conditions and their pressure derivatives at pressures below 42.6 GPa and above 58 GPa, respectively. The best fit yields $(\partial K_S/\partial P)_{300K}$ = 3.3 (±0.3), $(\partial \mu/\partial P)_{300K}$ = 1.91 (±0.02), with K_{S0} = 254 (±8) GPa, and μ_0 = 166.2 (±0.5) GPa below 42.6 GPa and $(\partial K_S/\partial P)_{300K}$ = 3.5 (±0.4), $(\partial \mu/\partial P)_{300K}$ = 1.54 (±0.11), with K_{S0} = 234 (±11) GPa, and μ_0 = 190.0 (±0.7) GPa above 58 GPa (Table S3). These aggregate elastic moduli behave quite differently in these two pressure ranges: μ shows a lower-pressure derivative for $P > 58$ GPa compared to $P < 42.6$ GPa, while K_S displays the opposite behavior (Figure 3).

Earlier studies have indicated that drastic softening of K_S and V_P could occur across the spin transition of Fe in lower-mantle Fe-bearing minerals, such as ferropericlase, magnesiosiderite, and the new hexagonal aluminous phase (Fu et al., 2017; Lin et al., 2013; Wu et al., 2013, 2016; Yang et al., 2015). Similarly, but distinct from the aforementioned Fe-bearing minerals, the spin and valence transitions of Fe in bridgmanite have been much debated due to its complicated crystal chemistry as well as the coupled substitution possibility of Al and Fe in crystallographic sites of bridgmanite (Catalli et al., 2010, 2011; Dorfman et al., 2015; Hsu et al., 2011; Lin et al., 2016; Mao et al., 2015). The current consensus is that both ferrous (Fe^{2+}) and ferric (Fe^{3+}) iron can be incorporated into bridgmanite, where Fe^{3+} can occupy both the large dodecahedral site (A site) and octahedral site (B site), while Fe^{2+} only occupies the A site (Lin et al., 2016; Mao et al., 2015; Shukla et al., 2016). In contrast, when Al^{3+} is incorporated into bridgmanite, Al^{3+} preferentially occupies the B site via a charge-coupled substitution in which Fe^{3+} enters the A site to replace Mg^{2+} (Hummer & Fei, 2012; Mao et al., 2017; Potapkin et al., 2013). A survey of recent theoretical and experimental studies indicates that B-site Fe^{3+} in bridgmanite will undergo a high-spin (HS) to low-spin transition at high pressures (Catalli et al., 2010; Hsu et al., 2011; Lin et al., 2012; Mao et al., 2015; Shukla et al., 2016). A noticeable volume collapse of ~0.5(±0.1)% has been observed across the spin transition between 18 and 25 GPa from P-V data at 300 K

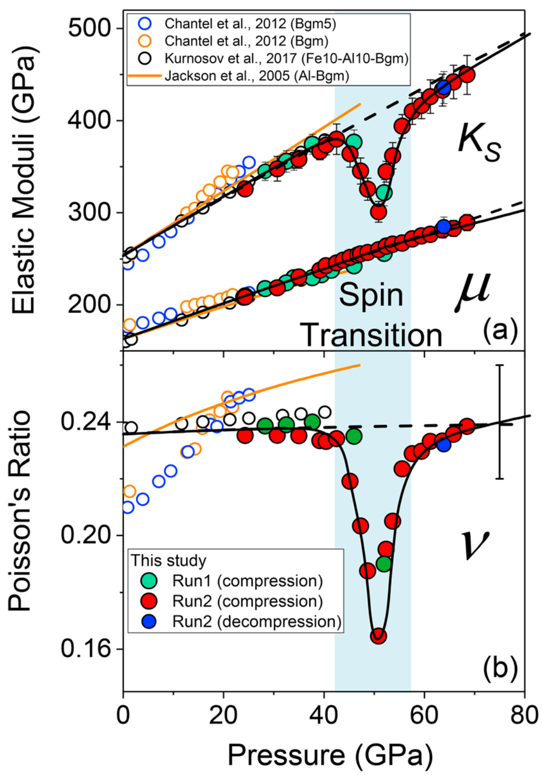

Figure 3. Elastic moduli and Poisson's ratio of polycrystalline bridgmanite $Mg_{0.96(1)}Fe^{2+}_{0.036(5)}Fe^{3+}_{0.014(5)}Si_{0.99(1)}O_3$ (Bgm5) at high pressures and 300 K. (a) Aggregate adiabatic bulk modulus (K_S) and shear modulus (μ), (b) Poisson's ratio (ν). Solid circles: experimental data from two runs; solid lines: best fits to experimental Run 2 data using thermoelastic equations (see supporting information for details); dashed lines: extrapolated results of high-spin bridgmanite from this study for comparison. The blue area represents the modeled spin transition region of B-site Fe^{3+} in Fe-bearing bridgmanite. Previous literature reports on bridgmanite with different compositions are also plotted for comparison. A representative error bar for the Poisson's ratio is plotted as a vertical line in the upper corner in Figure 3b. Uncertainties are smaller than symbols when not shown.

in bridgmanite with composition $(Mg_{0.9}Fe_{0.1})SiO_3$ containing 20% Fe^{3+} (Mao et al., 2015), and recent experimental study observed ~1.9% volume decrease within the spin transition of B-site Fe^{3+} in ferric-iron-only bridgmanite $(Mg_{0.46}Fe^{3+}_{0.53})(Fe^{3+}_{0.51}Si_{0.49})O_3$ (Liu et al., 2018). In contrast, both Fe^{3+} and Fe^{2+} in the A site have been reported to remain in the HS state throughout the entire lower-mantle pressure range (24–130 GPa) (Dorfman et al., 2015; Hsu et al., 2010, 2011; Lin et al., 2016). Additionally, A-site Fe^{2+} will undergo an enhanced lattice distortion at ~18–30 GPa, which results in extremely high quadrupole splitting (Catalli et al., 2010, 2011; Lin et al., 2012; McCammon et al., 2010; Narygina et al., 2010). The extremely high quadrupole splitting has alternatively been interpreted as the occurrence of the intermediate-spin state in bridgmanite (Hsu & Wentzcovitch, 2014; Lin et al., 2008; McCammon et al., 2008). Theoretical calculations have indicated that while A-site Fe^{2+} experiences lattice distortion in the HS state, the spin transition of B-site Fe^{3+} in bridgmanite would induce a volume reduction as well as a softening of V_P within the spin transition at 40–60 GPa (Hsu et al., 2011; Shukla et al., 2016). Analysis of the measured compression curve of Bgm5 from XRD data at 300 K also shows an abnormal reduction of ~0.8(±0.1)% in the unit cell volume between 44 and 61 GPa using the modeled EoS below 42.6 GPa as a reference (supporting information Figure S9). Considering the aforementioned discussion on the spin and valance states of Fe (both Fe^{2+} and Fe^{3+}) in bridgmanite at high pressure, together with the measured velocities and EoS of Bgm5, the observed V_P softening and normal V_S increase at ~42.6–58 GPa are most likely associated with a spin transition of B-site Fe^{3+}.

To explain the observed elasticity behavior in Bgm5 at high pressures, we followed a theoretical modeling approach (Fu et al., 2017; Shukla et al., 2016; Wu et al., 2013) to calculate the elastic properties of orthorhombic-structured bridgmanite across the spin transition of B-site Fe^{3+} at high pressure (see supporting information for details). We obtained remarkable consistency between experimental data and modeled results for V_P and V_S of Bgm5 across the spin transition (Figures 2 and 3). Compared to the extrapolated HS state, V_P is significantly softened by as much as ~6(±1)%, and K_S is softened by up to 25(±4)% across the spin transition. On the other hand, the change in V_S within V_P softening range is below the detection limit; hence, it appears to increase normally with increasing pressure. The observed softening of V_P in Bgm5 containing ~1.4 mol.% Fe^{3+} is comparable in magnitude to that of bridgmanite containing 5 mol.% B-site Fe^{3+} across the spin transition from ab initio calculations (Shukla et al., 2016). This indicates that a small amount of Fe^{3+} in bridgmanite undergoing a spin transition could significantly decrease V_P beyond current theoretical predictions. Furthermore, due to the decrease of V_P and normal increase in V_S in Bgm5 across the pressure range, the calculated Poisson's ratio, which is almost constant at ~0.24 at pressures below 42.6 and above 58 GPa, shows a significant reduction to a minimum value of 0.16 at approximately 52 GPa, midway within the V_P softening range.

To quantitatively understand the effects of Fe on the elasticity of bridgmanite at high pressures, we compared the measured density and velocities of Bgm5 in this study with those of pure $MgSiO_3$-bridgmanite (Figures 4, S10, and S11; Boffa Ballaran et al., 2012; Chantel et al., 2012; Karki et al., 1997; Murakami et al., 2007). At pressures below 42.6 GPa, V_P of Bgm5 is reduced by ~2–3% due to the substitution of 5 mol.% Fe in bridgmanite. Within the V_P softening range of 42.6–58 GPa, V_P of Bgm5 is ~10% lower than that of $MgSiO_3$-bridgmanite. At pressures above 58 GPa, bridgmanite shows velocity profiles distinct from those of extrapolated HS Bgm5. Specifically, V_P of Bgm5 is 1–2% lower than that of the extrapolated HS state.

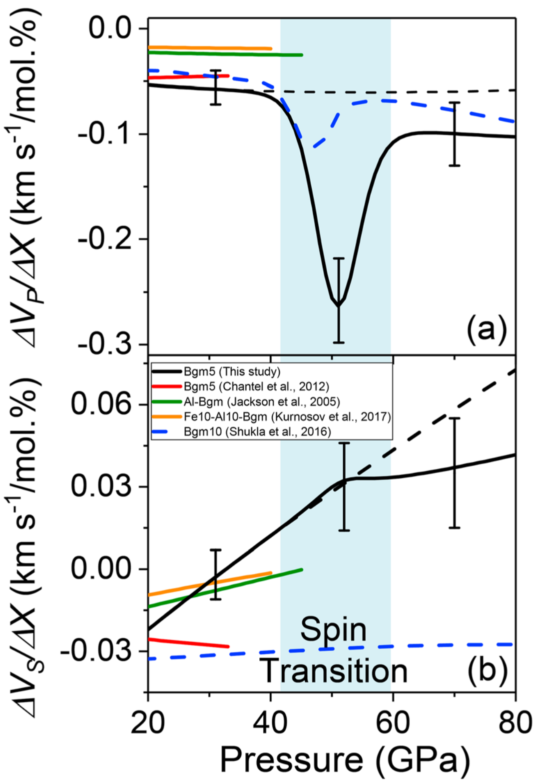

Figure 4. Variations of (a) compressional and (b) shear wave velocities with Fe and/or Al concentrations ($\Delta V_P/\Delta X$, $\Delta V_S/\Delta X$) in bridgmanite at high pressures and 300 K. X is the total Fe and Al content in bridgmanite in mole percent. V_P and V_S of pure-$MgSiO_3$ bridgmanite were used as a reference (Chantel et al., 2012; Murakami et al., 2007). Black dashed lines are extrapolated high-spin Bgm5 at high pressure for comparison. Literature experimental results on Fe-bearing bridgmanite [$Mg_{0.95}Fe^{2+}_{0.04}Fe^{3+}_{0.01}SiO_3$, Bgm5] (Chantel et al., 2012), Al-bearing bridgmanite containing 5.1 wt % Al_2O_3 (Jackson et al., 2005), and (Al,Fe)-bearing bridgmanite [$(Mg_{0.9}Fe_{0.1}Si_{0.9}Al_{0.1})O_3$, Fe10-Al10-Bgm] (Kurnosov et al., 2017) are also plotted for comparison. The blue dashed lines are from theoretical calculations on the spin transition of B-site Fe^{3+} in bridgmanite [$(Mg_{0.95}Fe_{0.05})(Si_{0.95}Fe_{0.05})O_3$, Bgm10] (Shukla et al., 2016). Blue areas represent the spin transition region of B-site Fe^{3+} in our sample. Vertical bars are shown as uncertainties from standard error propagation.

The modeled results in Figure 4 indicate that the incorporation of Fe in bridgmanite associated with a density increase would decrease V_P strongly with $\Delta V_P/\Delta Fe$ ~−0.05 km s^{-1}/mol.% for pressures below 42.6 GPa, ~−0.25 km s^{-1}/mol.% within the V_P softening range, and ~−0.1 km s^{-1}/mol.% for pressures above 58 GPa. On the other hand, the effects of Fe on V_S appear to vary significantly with pressure. V_S of Bgm5 decreases by ~1–2% below 30 GPa, while the effect of Fe on V_S gradually becomes positive with pressure, increasing up to 70 GPa. In particular, V_S of Bgm5 is elevated by as much as ~3(±1)% at pressures above 40 GPa compared to $MgSiO_3$-bridgmanite. As a result, a slightly increased V_S with $\Delta V_S/\Delta Fe$ of ~0.05 km s^{-1}/mol.% is expected at pressures above 40 GPa.

4. Geophysical Implication

The observed drastic decrease of V_P at 42.6–58 GPa and the increase of V_S with increasing Fe in bridgmanite can greatly affect the interpretation of seismological heterogeneities of the Earth's lower mantle. Tomographic modeling of lower-mantle seismic wave velocities indicates that some ancient subducted slabs could penetrate deeply into the lowermost mantle, displaying fast V_S (Masters et al., 2000; Shephard et al., 2017; Simmons et al., 2010). Subduction slabs tend to show notable V_P anomalies at a depth greater than ~1,500 km where V_P and V_S are not strongly correlated (Masters et al., 2000; Simmons et al., 2010). Furthermore, V_P and V_S show a weak and almost negative correlation with depths at ~2100 km. This seismic signature has been attributed to either chemical heterogeneities or lateral temperature variations coupled with a spin transition in lower-mantle minerals (Simmons et al., 2010; Wu & Wentzcovitch, 2017).

Previous studies have indicated that Al-depleted harzburgite or pyroxenite could be subducted into the lower mantle, enriching lower-mantle regions with Fe-rich and Al-depleted material (Irifune et al., 2010; Konter et al., 2016; Xu et al., 2008; Yoshida, 2013). Such chemically distinct Fe-rich, Al-depleted materials could produce Fe-bearing bridgmanite in the lower mantle that would be seismically distinct from (Al,Fe)-bearing bridgmanite with pyrolitic composition. Previous experimental data indicate that thermal effects at lower-mantle pressures would decrease both V_P and V_S of bridgmanite with $\partial V_P/\partial T \approx -2.8 \times 10^{-4}$ km/(s · K), $\partial V_S/\partial T \approx -2.3 \times 10^{-4}$ km/(s · K) (Figure S12; Chantel et al., 2012; Li & Zhang, 2005; Murakami et al., 2012). Therefore, V_S and V_P of Fe-bearing bridgmanite in colder ancient subducted slabs are expected to be higher than velocities of the averaged bulk mantle. Based on our study and recent theoretical predictions (Hsu et al., 2011; Shukla et al., 2016), the spin transition of B-site Fe^{3+} could affect the velocity profiles of Fe-bearing bridgmanite down to mid-lower mantle P-T conditions. As a result, the V_P increase due to relatively cold temperatures in Fe-rich subducted material could be canceled out by V_P softening arising from the spin transition of B-site Fe^{3+}, while the V_S increase would be magnified in these regions (Figure S13). Considering the broadened spin crossover pressures of B-site Fe^{3+} at elevated temperatures (Shukla et al., 2016), the magnitude of V_P softening might be reduced under lower-mantle P-T conditions. This could provide a plausible explanation for the seismically observed low correlation between V_P and V_S in subducted slabs in the mid-lower mantle caused by spin transition-induced seismic heterogeneities in Fe-bearing bridgmanite (Masters et al., 2000; Simmons et al., 2010). In comparison, the spin transition of B-site Fe^{3+} is not expected to occur in (Al,Fe)-bridgmanite in pyrolitic lower mantle due to the preferential substitution of Al^{3+} in the B site (Lin et al., 2016; Shukla et al., 2016). Therefore, normal V_P and V_S profiles in (Al,Fe)-bearing bridgmanite would be expected in the lower mantle. Furthermore, if low-spin Fe-bearing bridgmanite existed in deeper parts of the lower mantle, it would be manifested seismically by increased density and V_S but normal V_P and Poisson's ratio. These results challenge previously proposed iron enrichment models for the origin of LLSVPs that are seismically observed to have reduced V_S and increased density (Garnero et al., 2016; Lee et al., 2010). Further studies on the elasticity of (Al,Fe)-bearing bridgmanite and ferropericlase and associated iron partitioning at lower-mantle *P-T* conditions especially across their spin and valence transitions are needed to unravel the seismically inferred thermal and chemical heterogeneities of the Earth's lower mantle.

Acknowledgments
The authors thank V. Prakapenka and E. Greenberg for their assistance with X-ray diffraction experiments at 13ID-D, GSECARS. J. F. Lin acknowledges support from Geophysics, Instrumentation and Facilities, and CSEDI Programs of the U.S. National Science Foundation, the Visiting Professorship Program of the Institute for Planetary Materials, Okayama University, and Center for High Pressure Science and Technology Advanced Research (HPSTAR). T. Okuchi acknowledges support from JSPS KAKENHI (17H01172). GSECARS was supported by the National Science Foundation (EAR-0622171) and U.S. Department of Energy (DE-FG02-94ER14466) under contract DE-AC02-06CH11357. APS is supported by DOE-BES, under contract DE-AC02-06CH11357. Experimental sound velocity data from BLS and ISLS measurements and volume data from XRD results are listed in Tables S1 and S2, respectively. A more detailed discussion of the methodology can be found in the supporting information.

References

Badro, J., Fiquet, G., & Guyot, F. (2005). Thermochemical state of the lower mantle: New insights from mineral physics. In R. D. van der Hilst, et al. (Eds.), *Earth's Deep Mantle: Structure, Composition, and Evolution, Geophysical Monograph Series* (Vol. 160, pp. 241–260). Washington, DC: American Geophysical Union.

Boffa Ballaran, T., Kurnosov, A., Glazyrin, K., Frost, D. J., Merlini, M., Hanfland, M., & Caracas, R. (2012). Effect of chemistry on the compressibility of silicate perovskite in the lower mantle. *Earth and Planetary Science Letters*, *333*, 181–190.

Catalli, K., Shim, S.-H., Dera, P., Prakapenka, V. B., Zhao, J., Sturhahn, W., et al. (2011). Effects of the Fe^{3+} spin transition on the properties of aluminous perovskite—New insights for lower-mantle seismic heterogeneities. *Earth and Planetary Science Letters*, *310*(3-4), 293–302. https://doi.org/10.1016/j.epsl.2011.08.018

Catalli, K., Shim, S.-H., Prakapenka, V. B., Zhao, J., Sturhahn, W., Chow, P., et al. (2010). Spin state of ferric iron in $MgSiO_3$ perovskite and its effect on elastic properties. *Earth and Planetary Science Letters*, *289*(1-2), 68–75. https://doi.org/10.1016/j.epsl.2009.10.029

Chantel, J., Frost, D. J., McCammon, C. A., Jing, Z. C., & Wang, Y. B. (2012). Acoustic velocities of pure and iron-bearing magnesium silicate perovskite measured to 25 GPa and 1200 K. *Geophysical Research Letters*, *39*, L19307. https://doi.org/10.1029/2012GL053075

Davies, D. R., Goes, S., & Lau, H. C. P. (2015). Thermally dominated deep mantle LLSVPs: A review. In *The Earth's Heterogeneous Mantle* (Chap. 14, pp. 441–477). Switzerland: Springer Int. Publ.

Deschamps, F., Trampert, J., & Tackley, P. J. (2007). Thermo-chemical structure of the lower mantle: Seismological evidence and consequences for geodynamics. In *Superplumes: Beyond Plate Tectonics* (pp. 293–320). Netherlands: Springer.

Dewaele, A., Torrent, M., Loubeyre, P., & Mezouar, M. (2008). Compression curves of transition metals in the Mbar range: Experiments and projector augmented-wave calculations. *Physical Review B*, *78*(10), 104102. https://doi.org/10.1103/PhysRevB.78.104102

Dorfman, S. M., Badro, J., Rueff, P., Chow, P., Xiao, Y., & Gillet, P. (2015). Composition dependence of spin transition in (Mg,Fe)SiO_3 bridgmanite. *American Mineralogist*, *100*(10), 2246–2253. https://doi.org/10.2138/am-2015-5190

Dorfman, S. M., Meng, Y., Prakapenka, V. B., & Duffy, T. S. (2013). Effects of Fe-enrichment on the equation of state and stability of (Mg,Fe)SiO_3 perovskite. *Earth and Planetary Science Letters*, *361*, 249–257. https://doi.org/10.1016/j.epsl.2012.10.033

Fu, S., Yang, J., & Lin, J.-F. (2017). Abnormal elasticity of single-crystal magnesiosiderite across the spin transition in Earth's lower mantle. *Physical Review Letters*, *118*(3), 036402. https://doi.org/10.1103/PhysRevLett.118.036402

Fukui, H., Yoneda, A., Nakatsuka, A., Tsujino, N., Kamada, S., Ohtani, E., et al. (2016). Effect of cation substitution on bridgmanite elasticity: A key to interpret seismic anomalies in the lower mantle. *Scientific Reports*, *6*(1), 33337. https://doi.org/10.1038/srep33337

Garnero, E. J., Lay, T., & McNamara, A. (2007). Implications of lower-mantle structural heterogeneity for the existence and nature of whole-mantle plumes. *Geological Society of America Special Papers*, *430*, 79–101.

Garnero, E. J., & McNamara, A. K. (2008). Structure and dynamics of Earth's lower mantle. *Science*, *320*(5876), 626–628. https://doi.org/10.1126/science.1148028

Garnero, E. J., McNamara, A. K., & Shim, S.-H. (2016). Continent-sized anomalous zones with low seismic velocity at the base of Earth's mantle. *Nature Geoscience*, *9*(7), 481–489. https://doi.org/10.1038/ngeo2733

He, Y., & Wen, L. (2012). Geographic boundary of the "Pacific Anomaly" and its geometry and transitional structure in the north. *Journal of Geophysical Research*, *117*, B09308. https://doi.org/10.1029/2012JB009436

Hsieh, W. P., Deschamps, F., Okuchi, T., & Lin, J. F. (2017). Reduced lattice thermal conductivity of Fe-bearing bridgmanite in Earth's deep mantle. *Journal of Geophysical Research: Solid Earth*, *122*, 4900–4917. https://doi.org/10.1002/2017JB014339

Hsu, H., Blaha, P., Cococcioni, M., & Wentzcovitch, R. M. (2011). Spin-state crossover and hyperfine interactions of ferric iron in $MgSiO_3$ perovskite. *Physical Review Letters*, *106*(11), 118501. https://doi.org/10.1103/PhysRevLett.106.118501

Hsu, H., Umemoto, K., Blaha, P., & Wentzcovitch, R. M. (2010). Spin states and hyperfine interactions of iron in (Mg,Fe)SiO_3 perovskite under pressure. *Earth and Planetary Science Letters*, *294*(1-2), 19–26. https://doi.org/10.1016/j.epsl.2010.02.031

Hsu, H., & Wentzcovitch, R. M. (2014). First-principles study of intermediate-spin ferrous iron in the Earth's lower mantle. *Physical Review B*, *90*(19), 195205. https://doi.org/10.1103/PhysRevB.90.195205

Hummer, D. R., & Fei, Y. (2012). Synthesis and crystal chemistry of Fe^{3+}-bearing (Mg,Fe^{3+})(Si,Fe^{3+})O_3 perovskite. *American Mineralogist*, *97*(11–12), 1915–1921. https://doi.org/10.2138/am.2012.4144

Irifune, T., Shinmei, T., McCammon, C. A., Miyajima, N., Rubie, D. C., & Frost, D. J. (2010). Iron partitioning and density changes of pyrolite in Earth's lower mantle. *Science*, *327*(5962), 193–195. https://doi.org/10.1126/science.1181443

Jackson, J. M., Zhang, J., Shu, J., Sinogeikin, S. V., & Bass, J. D. (2005). High-pressure sound velocities and elasticity of aluminous $MgSiO_3$ perovskite to 45 GPa: Implications for lateral heterogeneity in Earth's lower mantle. *Geophysical Research Letters*, *32*, L21305. https://doi.org/10.1029/2005GL023522

Karato, S. i., & Karki, B. B. (2001). Origin of lateral variation of seismic wave velocities and density in the deep mantle. *Journal of Geophysical Research*, *106*, 21,771–21,783. https://doi.org/10.1029/2001JB000214

Karki, B., Stixrude, L., Clark, S., Warren, M., Ackland, G., & Crain, J. (1997). Elastic properties of orthorhombic $MgSiO_3$ perovskite at lower mantle pressures. *American Mineralogist*, *82*(5-6), 635–638. https://doi.org/10.2138/am-1997-5-623

Kesson, S., Gerald, J. F., & Shelley, J. (1998). Mineralogy and dynamics of a pyrolite lower mantle. *Nature*, *393*(6682), 252–255. https://doi.org/10.1038/30466

Konter, J. G., Pietruszka, A. J., Hanan, B. B., Finlayson, V. A., Craddock, P. R., Jackson, M. G., & Dauphas, N. (2016). Unusual δ^{56}Fe values in Samoan rejuvenated lavas generated in the mantle. *Earth and Planetary Science Letters*, *450*, 221–232. https://doi.org/10.1016/j.epsl.2016.06.029

Kurnosov, A., Marquardt, H., Frost, D., Ballaran, T. B., & Ziberna, L. (2017). Evidence for a Fe^{3+}−rich pyrolitic lower mantle from (Al, Fe)-bearing bridgmanite elasticity data. *Nature*, *543*(7646), 543–546. https://doi.org/10.1038/nature21390

Lee, C.-T. A., Luffi, P., Höink, T., Li, J., Dasgupta, R., & Hernlund, J. (2010). Upside-down differentiation and generation of a 'primordial' lower mantle. *Nature*, *463*(7283), 930–933. https://doi.org/10.1038/nature08824

Li, B. S., & Zhang, J. Z. (2005). Pressure and temperature dependence of elastic wave velocity of $MgSiO_3$ perovskite and the composition of the lower. *Physics of the Earth and Planetary Interiors*, *151*(1–2), 143–154. https://doi.org/10.1016/j.pepi.2005.02.004

Lin, J. F., Alp, E. E., Mao, Z., Inoue, T., McCammon, C., Xiao, Y., et al. (2012). Electronic spin states of ferric and ferrous iron in the lower-mantle silicate perovskite. *American Mineralogist*, *97*(4), 592–597. https://doi.org/10.2138/am.2012.4000

Lin, J. F., Mao, Z., Yang, J., Liu, J., Xiao, Y. M., Chow, P., & Okuchi, T. (2016). High-spin Fe^{2+} and Fe^{3+} in single-crystal aluminous bridgmanite in the lower mantle. *Geophysical Research Letters*, *43*, 6952–6959. https://doi.org/10.1002/2016GL069836

Lin, J. F., Speziale, S., Mao, Z., & Marquardt, H. (2013). Effects of the electronic spin transitions of Iron in lower mantle minerals: Implications for deep mantle geophysics and geochemistry. *Reviews of Geophysics*, *51*, 244–275. https://doi.org/10.1002/rog.20010

Lin, J. F., Watson, H., Vankó, G., Alp, E. E., Prakapenka, V. B., Dera, P., et al. (2008). Intermediate-spin ferrous iron in lowermost mantle post-perovskite and perovskite. *Nature Geoscience*, *1*(10), 688–691. https://doi.org/10.1038/ngeo310

Liu, J., Dorfman, S. M., Zhu, F., Li, J., Wang, Y., Zhang, D., et al. (2018). Valence and spin states of iron are invisible in Earth's lower mantle. *Nature Communications*, *9*(1), 1284. https://doi.org/10.1038/s41467-018-03671-5

Lundin, S., Catalli, K., Santillan, J., Shim, S. H., Prakapenka, V. B., Kunz, M., & Meng, Y. (2008). Effect of Fe on the equation of state of mantle silicate perovskite over 1 Mbar. *Physics of the Earth and Planetary Interiors*, *168*(1–2), 97–102. https://doi.org/10.1016/j.pepi.2008.05.002

Mao, H. K., Xu, J., & Bell, P. M. (1986). Calibration of the ruby pressure gauge to 800-Kbar under quasi-hydrostatic conditions. *Journal of Geophysical Research*, *91*, 4673–4676. https://doi.org/10.1029/JB091iB05p04673

Mao, Z., Lin, J. F., Yang, J., Inoue, T., & Prakapenka, V. B. (2015). Effects of the Fe^{3+} spin transition on the equation of state of bridgmanite. *Geophysical Research Letters*, *42*, 4335–4342. https://doi.org/10.1002/2015GL064400

Mao, Z., Wang, F., Lin, J.-F., Fu, S., Yang, J., Wu, X., et al. (2017). Equation of state and hyperfine parameters of high-spin bridgmanite in the Earth's lower mantle by synchrotron X-ray diffraction and Mössbauer spectroscopy. *American Mineralogist*, *102*(2), 357–368. https://doi.org/10.2138/am-2017-5770

Masters, G., Laske, G., Bolton, H., & Dziewonski, A. (2000). The relative behavior of shear velocity, bulk sound speed, and compressional velocity in themantle: Implications for chemical and thermal structure. In S. Karato, et al. (Eds.), *Earth's Deep Interior: Mineral Physics and Tomography Fromthe Atomic to the Global Scale, Geophysical Monograph Series* (Vol. 117, pp. 63–87). Washington, DC: American Geophysical Union.

McCammon, C., Dubrovinsky, L., Narygina, O., Kantor, I., Wu, X., Glazyrin, K., et al. (2010). Low-spin Fe^{2+} in silicate perovskite and a possible layer at the base of the lower mantle. *Physics of the Earth and Planetary Interiors*, *180*(3-4), 215–221. https://doi.org/10.1016/j.pepi.2009.10.012

McCammon, C., Kantor, I., Narygina, O., Rouquette, J., Ponkratz, U., Sergueev, I., et al. (2008). Stable intermediate-spin ferrous iron in lower-mantle perovskite. *Nature Geoscience*, *1*(10), 684–687. https://doi.org/10.1038/ngeo309

Murakami, M., Ohishi, Y., Hirao, N., & Hirose, K. (2012). A perovskitic lower mantle inferred from high-pressure, high-temperature sound velocity data. *Journal of the Geological Society of India*, *80*(1), 147–147. https://doi.org/10.1007/s12594-012-0111-2

Murakami, M., Sinogeikin, S. V., Hellwig, H., Bass, J. D., & Li, J. (2007). Sound velocity of $MgSiO_3$ perovskite to Mbar pressure. *Earth and Planetary Science Letters*, *256*(1-2), 47–54. https://doi.org/10.1016/j.epsl.2007.01.011

Narygina, O. V., Kantor, I. Y., McCammon, C., & Dubrovinsky, L. (2010). Electronic state of Fe^{2+} in (Mg,Fe)(Si,Al)O_3 perovskite and (Mg,Fe)SiO_3 majorite at pressures up to 81 GPa and temperatures up to 800 K. *Physics and Chemistry of Minerals*, *37*(6), 407–415. https://doi.org/10.1007/s00269-009-0342-y

Potapkin, V., McCammon, C., Glazyrin, K., Kantor, A., Kupenko, I., Prescher, C., et al. (2013). Effect of iron oxidation state on the electrical conductivity of the Earth's lower mantle. *Nature Communications*, *4*, 1427. https://doi.org/10.1038/ncomms2436

Ringwood, A. E. (1975). *Composition and petrology of the Earth's mantle* (1st ed., 672 pp.). New York: McGraw-Hill.

Shephard, G. E., Matthews, K. J., Hosseini, K., & Domeier, M. (2017). On the consistency of seismically imaged lower mantle slabs. *Scientific Reports Uk*, *7*(1), 10976. https://doi.org/10.1038/s41598-017-11039-w

Shukla, G., Cococcioni, M., & Wentzcovitch, R. M. (2016). Thermoelasticity of Fe^{3+}-and Al-bearing bridgmanite: Effects of iron spin crossover. *Geophysical Research Letters*, *43*, 5661–5670. https://doi.org/10.1002/2016GL069332

Simmons, N. A., Forte, A. M., Boschi, L., & Grand, S. P. (2010). GyPSuM: A joint tomographic model of mantle density and seismic wave speeds. *Journal of Geophysical Research*, *115*, B12310. https://doi.org/10.1029/2010JB007631

Tanaka, S., Suetsugu, D., Shiobara, H., Sugioka, H., Kanazawa, T., Fukao, Y., et al. (2009). On the vertical extent of the large low shear velocity province beneath the South Pacific Superswell. *Geophysical Research Letters*, *36*, L07305. https://doi.org/10.1029/2009GL037568

Trampert, J., Deschamps, F., Resovsky, J., & Yuen, D. (2004). Probabilistic tomography maps chemical heterogeneities throughout the lower mantle. *Science*, *306*(5697), 853–856. https://doi.org/10.1126/science.1101996

van der Hilst, R. D., & Kárason, H. (1999). Compositional heterogeneity in the bottom 1000 kilometers of Earth's mantle: Toward a hybrid convection model. *Science*, *283*(5409), 1885–1888. https://doi.org/10.1126/science.283.5409.1885

Wentzcovitch, R., Karki, B., Cococcioni, M., & De Gironcoli, S. (2004). Thermoelastic properties of $MgSiO_3$-perovskite: Insights on the nature of the Earth's lower mantle. *Physical Review Letters*, *92*(1), 018501. https://doi.org/10.1103/PhysRevLett.92.018501

Wolf, A. S., Jackson, J. M., Dera, P., & Prakapenka, V. B. (2015). The thermal equation of state of (Mg,Fe)SiO_3 bridgmanite (perovskite) and implications for lower mantle structures. *Journal of Geophysical Research: Solid Earth*, *120*, 7460–7489. https://doi.org/10.1002/2015JB012108

Wu, Y., Wu, X., Lin, J. F., McCammon, C. A., Xiao, Y. M., Chow, P., et al. (2016). Spin transition of ferric iron in the NAL phase: Implications for the seismic heterogeneities of subducted slabs in the lower mantle. *Earth and Planetary Science Letters*, *434*, 91–100. https://doi.org/10.1016/j.epsl.2015.11.011

Wu, Z., & Wentzcovitch, R. M. (2017). Composition versus temperature induced velocity heterogeneities in a pyrolitic lower mantle. *Earth and Planetary Science Letters*, *457*, 359–365. https://doi.org/10.1016/j.epsl.2016.10.009

Wu, Z. Q., Justo, J. F., & Wentzcovitch, R. M. (2013). Elastic anomalies in a spin-crossover system: Ferropericlase at lower mantle conditions. *Physical Review Letters*, *110*(22). https://doi.org/10.1103/PhysRevLett.110.228501

Xu, S., Lin, J. F., & Morgan, D. (2017). Iron partitioning between ferropericlase and bridgmanite in the Earth's lower mantle. *Journal of Geophysical Research: Solid Earth*, *122*, 1074–1087. https://doi.org/10.1002/2016JB013543

Xu, W., Lithgow-Bertelloni, C., Stixrude, L., & Ritsema, J. (2008). The effect of bulk composition and temperature on mantle seismic structure. *Earth and Planetary Science Letters*, *275*(1-2), 70–79. https://doi.org/10.1016/j.epsl.2008.08.012

Yang, J., Tong, X., Lin, J. F., Tomioka, N., Okuchi, T., & Prakapenka, V. B. (2015). Elasticity of ferropericlase across the spin crossover in the Earth's lower mantle. *Scientific Reports*, *5*, 7188.

Yoshida, M. (2013). The role of harzburgite layers in the morphology of subducting plates and the behavior of oceanic crustal layers. *Geophysical Research Letters*, *40*, 5387–5392. https://doi.org/10.1002/2013GL057578